

# Experimental investigation on tribological behaviours of PA6, PA6-reinforced Al<sub>2</sub>O<sub>3</sub> and PA6-reinforced graphite polymer composites

S SATHEESKUMAR<sup>1</sup> and G KANAGARAJ<sup>2,\*</sup>

<sup>1</sup>Department of Mechanical Engineering, Lathamathavan Engineering College, Madurai 625 301, India

<sup>2</sup>Department of Mechanical Engineering, Thiagarajar College of Engineering, Madurai 625 015, India

MS received 3 September 2015; accepted 7 April 2016

**Abstract.** This article reports on the preparation, characterization and experimental investigation of polyamide 6 (PA6) reinforced with alumina oxide (Al<sub>2</sub>O<sub>3</sub>) and graphite composites. The test specimens were prepared in an injection-moulding machine by varying the weight proportions of Al<sub>2</sub>O<sub>3</sub> and graphite particles blended with PA6. The tribological properties of the composites were observed by using pin-on-disc wear test rig under dry sliding conditions. The worn surfaces of the composites were examined using scanning electron microscope. The addition of Al<sub>2</sub>O<sub>3</sub> and graphite significantly enhanced the tribological properties of PA6. The PA6 containing 30 wt% Al<sub>2</sub>O<sub>3</sub> and 20 wt% graphite revealed the best tribological behaviours due to the stronger interfacial bonding characteristics with improved wear resistance. Further, the thermal stability of Al<sub>2</sub>O<sub>3</sub> and graphite particles was studied through thermogravimetric analysis test. It was also found that further addition of Al<sub>2</sub>O<sub>3</sub> and graphite in PA6 had no significant improvement in wear resistance, the co-efficient of friction and heat generation.

**Keywords.** Al<sub>2</sub>O<sub>3</sub>; graphite; friction; reinforcement; PA6; wear.

## 1. Introduction

Demands for engineering plastics that replace metal parts are increasing in recent years in order to reduce the weight and increase the productivity of metal components for various applications. However, limitations in mechanical and tribological properties, the low heat deflection temperature, high water absorption and dimensional instability of pure PA6 have prevented its wide range of applications. To overcome this difficulty, many researchers paid attention and improved the property of PA6 significantly by reinforcement methods. Reinforcements are usually done to improve the properties of the base metals like strength, stiffness, conductivity, etc. Al<sub>2</sub>O<sub>3</sub> has been widely used as filler material in high-performance materials to increase ductility, scratch resistance and toughness. Al<sub>2</sub>O<sub>3</sub> particles have excellent wear and corrosion resistance in a wide range of environments and temperatures, higher strength-to-weight ratio and higher strength retention at elevated temperature. Graphite has been widely used as filler material in high-performance materials to increase compressive strength and high thermal conductivity. Graphite particles have excellent lubricity, corrosion and hot shock resistance in a wide range of environments and temperatures, higher strength-to-weight ratio and higher strength retention at elevated temperature. In this article, the tribological properties of PA6, Al<sub>2</sub>O<sub>3</sub> and graphite particles reinforced with different compositions were examined.

The mechanical and tribological behaviour of polyamide, high-density polyethylene and their composites have been studied and reported in the literature [1–3]. Many researchers paid attention to improving the property of PA6 significantly by using reinforcement methods. The original PA6 material without reinforcement is known as matrix. Reinforcements are usually done by adding solid lubricants, fillers, metals, ceramics and additive materials to improve the property of the base metals in terms of strength, stiffness and conductivity.

Kukureka and group [4,5] investigated the friction and wear tests for aramid, carbon and glass fibre composites running against identical materials in a twin disc machine. Carbon and glass fibres significantly reduce the co-efficient of friction and this enables the contact to carry higher loads and slips before the melting point of the matrix is reached. Palabiyik and Bahadur [6] studied the structure and the mechanical and tribological properties of PA6 and high-density polyethylene poly blends with and without the compatibilizing agent maleic anhydride propylene and they found that the best co-efficient of friction and high wear resistance were identified at 60 wt% PA6–40 wt% HDPE and 80 wt% PA6–20 wt% HDPE. Further, they investigated [7] PA6 and HDPE poly blend compositions of 80 wt% PA6–20 wt% HDPE and 60 wt% PA6–40 wt% HDPE on mechanical and tribological behaviour. The resultant poly blends were reinforced with glass fibre and filled PTFE and copper oxide. The maximum reduction in wear and the co-efficient of friction were obtained by filling the poly blends with 10 wt%

\* Author for correspondence (gkmech@tce.edu)

PTFE. Liu *et al* [8] inspected the dry sliding and lubricated friction and wear behaviours of PA and ultra-high molecular weight polyethylene (UHMWPE) blend. The tribological performance of PA and UHMWPE was also investigated for the purpose of comparison. The above three materials was compared, the PA demonstrated the highest co-efficient of friction and UHMWPE the lowest co-efficient of friction in dry sliding and lubricated test conditions.

Jia *et al* [9] conducted wear test and friction co-efficients of PTFE, PA66 and PPS self-mated couples under liquid paraffin lubrication, resulting in decrease by one order of magnitude compared with those under dry friction condition. They concluded that liquid paraffin decreases the wear of PTFE and PPS, while increases the wear of PA66. Cong and group [10] prepared PA46/HDPE poly blends with different volume ratios of 8/2, 6/4, 4/6 and 2/8. From their test results, they concluded that HDPE efficiently reduced the friction co-efficient of PA46. The friction co-efficients of all PA46/HDPE blends were as low as 0.21–0.22, which were near the friction co-efficient of pure HDPE, and much lower than that of pure PA46.

Li *et al* [11] examined reinforced PA6 with polyurethane (PA6–PU) block copolymers in different short glass proportions. When the addition of glass fibre content was 5%, the co-efficient of friction decreased to 30% and wear rate decreased to 68%. Liu and group [12] presented the effects of incorporated montmorillonite (MMT) on a surface and the mechanical properties of synthesized PA6/MMT composites that were prepared by the twin screw extruder mixer technique. The incorporation of MMT's (except 5 wt%) into PA6 might effectively enhance the wear resistance of PA6. Unal *et al* [13] examined the friction and wear characteristics of 5 wt% pure PA6, 15 wt% graphite-filled PA6 and 4 wt% wax-filled PA6 sliding against stainless steel under dry sliding conditions. The lowest wear rate was observed for 4 wt% wax-filled PA6 composites and the higher rate was achieved for pure PA6.

Pogacnik and kalin [14] focused on the parameters affecting the running in and long-term behaviour of plastic/plastic and plastic/steel contacts at sliding conditions. A smooth polymer disc surface causes a higher co-efficient of friction and high wear rates compared to a rough disc surface. For PA6/steel contacts, only a little plastic deformation with smearing was observed on the PA6 pin surfaces at high speeds, much less than for the PA6/POM contacts. Pan *et al* [15] analysed the mechanical and tribological properties of MC nylon/graphene oxide nanocomposites and they found that the nanocomposites have lower wear rates in comparison with MC nylon.

Li *et al* [16] investigated the tribological properties of the glass fibre-reinforced PA6 (GF/PA6, 15/85 by weight) for high-performance frictional materials using single or combinative solid lubricants, such as PTFE, UHMWPE and their combination. The combination of solid lubricants shows interaction effect on the reducing friction co-efficient at 12 wt% PTFE and 3 wt% UHMWPE. Shaofeng Zhou *et al* [17] studied the effect of carbon fibre reinforcement on mechanical and tribological properties of PA6/PPS polymer-based composites. The wear resistance of PA6/PPS–CF behaved better, as the content of carbon fibre increased.

From the literature review, there are only very few articles published on PA6 with other reinforced composites. In this study, the tribological behaviours of PA6, PA6 reinforced with Al<sub>2</sub>O<sub>3</sub> and PA6 reinforced with graphite in various weight proportions were carefully investigated in order to provide some practical guidance for the use of polymer-based composites.

## 2. Experimental

### 2.1 Chemicals and instrumentation

The density and melting temperature for PA6 were 1.14 g cm<sup>-3</sup> and 220°C, respectively. PA6 were purchased as pellets of size 3 mm and Al<sub>2</sub>O<sub>3</sub> particles of size 150 mesh, 88 micron and 0.0035 inches. Graphite fine powder purchased was of 60 mesh. The test specimens were prepared using an injection moulding machine with maximum chamber capacity of 150 g. The muffle furnace was supplied by M/s Prabha Machine Tools, Coimbatore, Tamilnadu, India.

Chemical composition of PA6 is represented in figure 1. This particular polyamide is called PA6, because it is formed from the polymerization of 6-aminohexanoic acid, a compound that contains 6 carbons. The starting material for PA6 is ε-caprolactum. The lactum is opened by hydrolysis.

### 2.2 Preparation process of PA6 and PA6-reinforced polymer composites

In order to evaluate the tribological properties of Al<sub>2</sub>O<sub>3</sub> blended with PA6 and graphite blended with PA6 composites, the PA6 composite blends were produced in different weight proportions of 5, 10, 20, and 30% Al<sub>2</sub>O<sub>3</sub> or graphite. The blending of Al<sub>2</sub>O<sub>3</sub> and graphite particles directly with PA6 is not easy because Al<sub>2</sub>O<sub>3</sub> and graphite particles have a high melting point temperature. Hence, before blending with PA6 they were preheated below its melting point temperature.

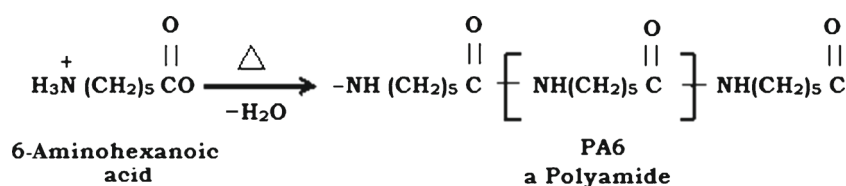


Figure 1. Chemical composition of PA6.

The preheating process was done in a muffle furnace, which is maintained at 1970°C for Al<sub>2</sub>O<sub>3</sub> and 2320°C for graphite. The preheated Al<sub>2</sub>O<sub>3</sub> and graphite were blended with PA6 by stirring process. Afterward the blended Al<sub>2</sub>O<sub>3</sub>, graphite, and PA6 are put into the injection moulding machine up to 50 min. The blended material was melted at a temperature of up to 220°C in an injection moulding machine. Simultaneously, the moulding die was preheated up to 75°C for the free flow of melted composites. At the temperature of 75°C, the die was inserted at the bottom of the injection moulding machine. The blended material was passed from injection moulding to die. The blended materials were formed as per ASTM standard of varying proportions by weight. The preparation process of PA6-reinforced polymer composites is shown in figure 2.

### 2.3 Specification of the composites

The tribological properties were conducted on a TR-20LE-PHM-400, DUCOM tribometer, Ducom Instruments, Bangalore, India. The test specimens were shaped for ASTM G99 and machined as 12 mm diameter and 30 mm length. In order to obtain an accurate value for weight loss, the samples were placed in an atmospheric air for 240 h for removing the moisture content. The weights of filler material were measured using precision electronic balance. The composite specimens Al<sub>2</sub>O<sub>3</sub>/PA6 and graphite/PA6 are shown in figures 3 and 4. The specimens for tribological tests were moulded in the

following composition (given in weight%) using an injection moulding machine.

- 100 wt% PA6
- 95 wt% PA6 + 5 wt% Al<sub>2</sub>O<sub>3</sub>
- 90 wt% PA6 + 10 wt% Al<sub>2</sub>O<sub>3</sub>
- 80 wt% PA6 + 20 wt% Al<sub>2</sub>O<sub>3</sub>
- 70 wt% PA6 + 30 wt% Al<sub>2</sub>O<sub>3</sub>
- 95 wt% PA6 + 5 wt% Gr
- 90 wt% PA6 + 10 wt% Gr
- 80 wt% PA6 + 20 wt% Gr
- 70 wt% PA6 + 30 wt% Gr

### 2.4 Testing conditions

Prior to the test, the test specimens were cleaned with methanol to remove the possible impurities on the surface. The speed was maintained in the range of 1000, 1500 and 2000 r.p.m. Then the load was applied in the range 5, 10, 20 and 30 N. Throughout the test, the wear process was carefully observed and the friction and wear data were collected by data acquisition system, which was stored and exhibited on a computer screen. The friction and wear characteristics were performed for five specimens by Pin-on-disc tribometer under different dry friction conditions at the room temperature. Here, the following constraints and test conditions were used in the pin-on-disc testing machine as shown in tables 1 and 2.

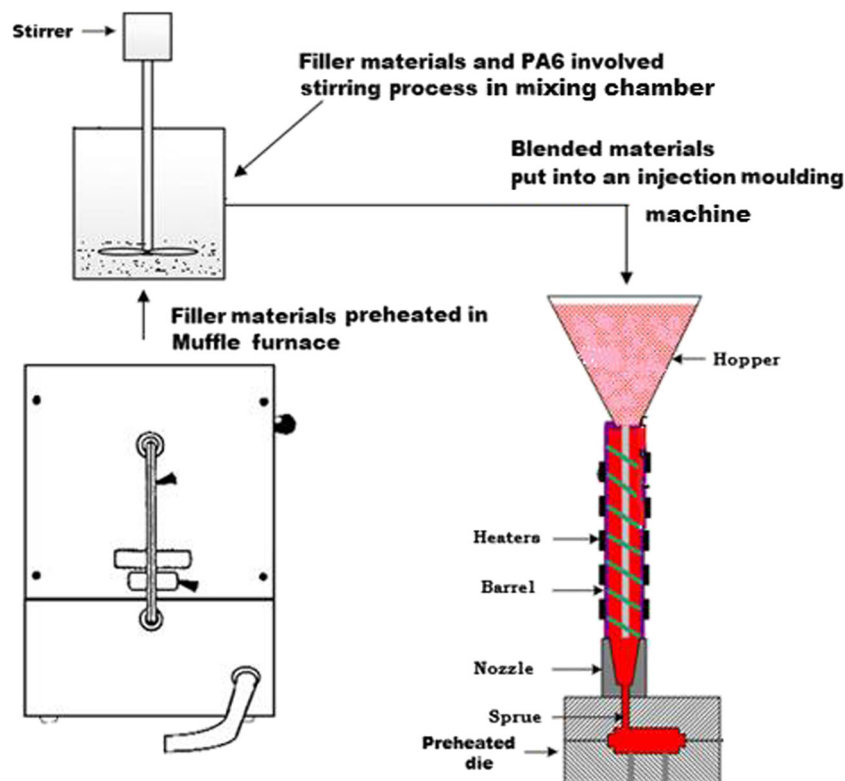


Figure 2. Preparation process of PA6 polymer composites.



**Figure 3.** PA6 and PA6 with Al<sub>2</sub>O<sub>3</sub> test specimens.



**Figure 4.** PA6 and PA6 with graphite test specimens.

**Table 1.** Testing conditions of Al<sub>2</sub>O<sub>3</sub>-reinforced PA6 composites.

Test specimen	Constraints	Testing conditions
PA6	Load	5, 10, 20 and 30 N
PA6 + 5 wt% Al <sub>2</sub> O <sub>3</sub>	Speed	1000–2000 r.p.m.
PA6 + 10 wt% Al <sub>2</sub> O <sub>3</sub>	Pin materials	PA6 with Al <sub>2</sub> O <sub>3</sub>
PA6 + 20 wt% Al <sub>2</sub> O <sub>3</sub>	Surface condition	Dry friction
PA6 + 30 wt% Al <sub>2</sub> O <sub>3</sub>	Track diameter	100 mm
	Disc material	EN31 steel
	Sliding distance	1000 m

**Table 2.** Testing conditions of graphite-reinforced PA6 composites.

Test specimen	Constraints	Testing conditions
PA6	Load	5, 10, 20 and 30 N
PA6 + 5 wt% graphite	Speed	1000–2000 r.p.m.
PA6 + 10 wt% graphite	Pin materials	PA6 with graphite
PA6 + 20 wt% graphite	Surface condition	Dry friction
PA6 + 30 wt% graphite	Track diameter	100 mm
	Disc material	EN31 steel
	Sliding distance	1000 m

### 2.5 Chemical composition of EN31 carbon steel

EN31 steel is a plain carbon steel; case hardened 65 HRC as provided with the pin-on-disc machine. The chemical composition is 0.9–1.20% C, 0.30–0.75% Mn, 0.050% S, 0.050% P, 0.10–0.35% SiC, 1.00–1.60% Cr.

### 2.6 SEM analysis of before and after worn surfaces of Al<sub>2</sub>O<sub>3</sub>-reinforced PA6 composites

Figure 5a and b shows the morphological image of pure PA6 test specimen of before and after worn surfaces. Figure 5a indicates some broken particles and plastic deformation

observed before wear of unreinforced PA6. In figure 5b, the wedge formation and plastic deformation were developed on the surfaces with more voids and microcracks found after wear of pure PA6. In figure 5c and d, Al<sub>2</sub>O<sub>3</sub> particles were uniformly dispersed in PA6. At the same time, PA6 with 5 wt% Al<sub>2</sub>O<sub>3</sub> depicts the plastic deformation and voids appear less compared with pure PA6 with 5 wt% Al<sub>2</sub>O<sub>3</sub>. Broken particles, microcracks and wedge formation were not exposed on the surface of PA6 with 5 wt% Al<sub>2</sub>O<sub>3</sub>. Figure 5e represents the voids formation and broken particles, while figure 5f shows the voids formation, plastic deformation and broken particles of PA6 with 10 wt% Al<sub>2</sub>O<sub>3</sub>. It is hard to disperse Al<sub>2</sub>O<sub>3</sub> particles uniformly in the PA6 composite.



Figure 5g and h shows the image of 20 wt%  $\text{Al}_2\text{O}_3$ , this image clearly depicts the uniform distribution of  $\text{Al}_2\text{O}_3$  particles in PA6. At the same time, plastic deformation and broken particles were formed on the before worn surfaces. Additional microcracks were found on the surfaces of PA6, as in figure 5h. Figure 5i shows the voids formation, plastic deformation and broken particles of PA6 with 30 wt%  $\text{Al}_2\text{O}_3$ . Additionally, the image depicts the crest formation on the PA6. Figure 5j shows the sponginess because of after wear of the PA6 surface, the bonding of  $\text{Al}_2\text{O}_3$  particles are not evenly scattered at various surfaces.

These image shows the increase of  $\text{Al}_2\text{O}_3$  with PA6, the porosity of the  $\text{Al}_2\text{O}_3$  material as captured in the PA6. Wear direction is also clearly visible in figure 5j. It reveals that higher wear occurred on PA6 with 30 wt%  $\text{Al}_2\text{O}_3$ . The worn surface of the composite was very smooth and there appeared

more integrated wear debris oriented along the sliding direction. It is noted that  $\text{Al}_2\text{O}_3$  reinforced with PA6 surfaces usually wear more quickly. The more amount of porous of  $\text{Al}_2\text{O}_3$  is blended with PA6, as comparatively higher as the previous composition. It is seen that the dispersion condition of  $\text{Al}_2\text{O}_3$  in the PA6 matrix are reasonably uniform in the 30 wt% composites. In summary, the uniform distribution of  $\text{Al}_2\text{O}_3$  particles in the microstructure of PA6 material is the major responsible factor for the improvement in the tribological properties.

### 2.7 SEM analysis of before and after worn surface of PA6- and graphite-reinforced PA6 composites

Figure 6a and b reveals the morphological image of pure PA6 test specimen before and after worn surfaces. In figure 6c, the

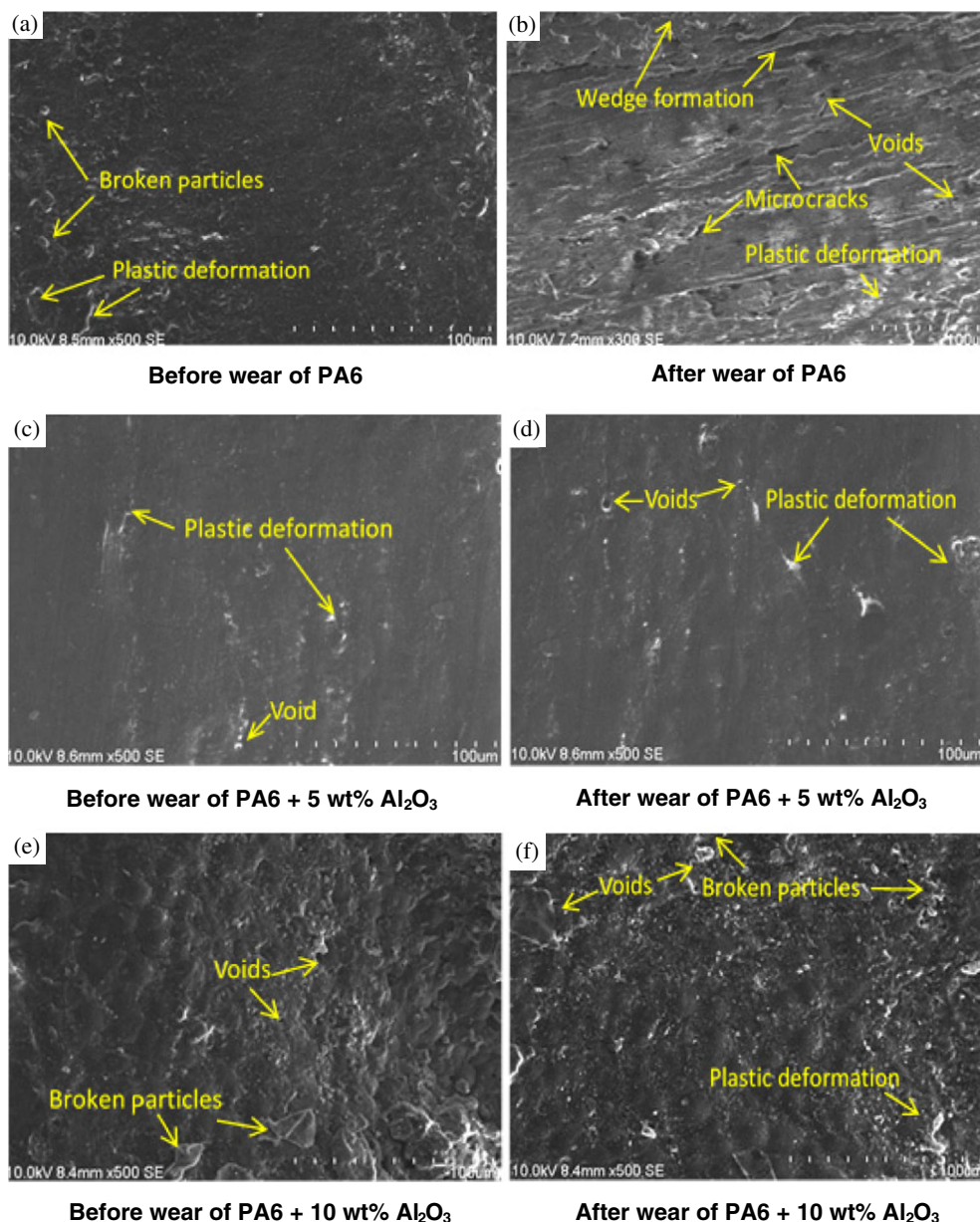


Figure 5. SEM images of PA6 and  $\text{Al}_2\text{O}_3$ -reinforced PA6 composites.

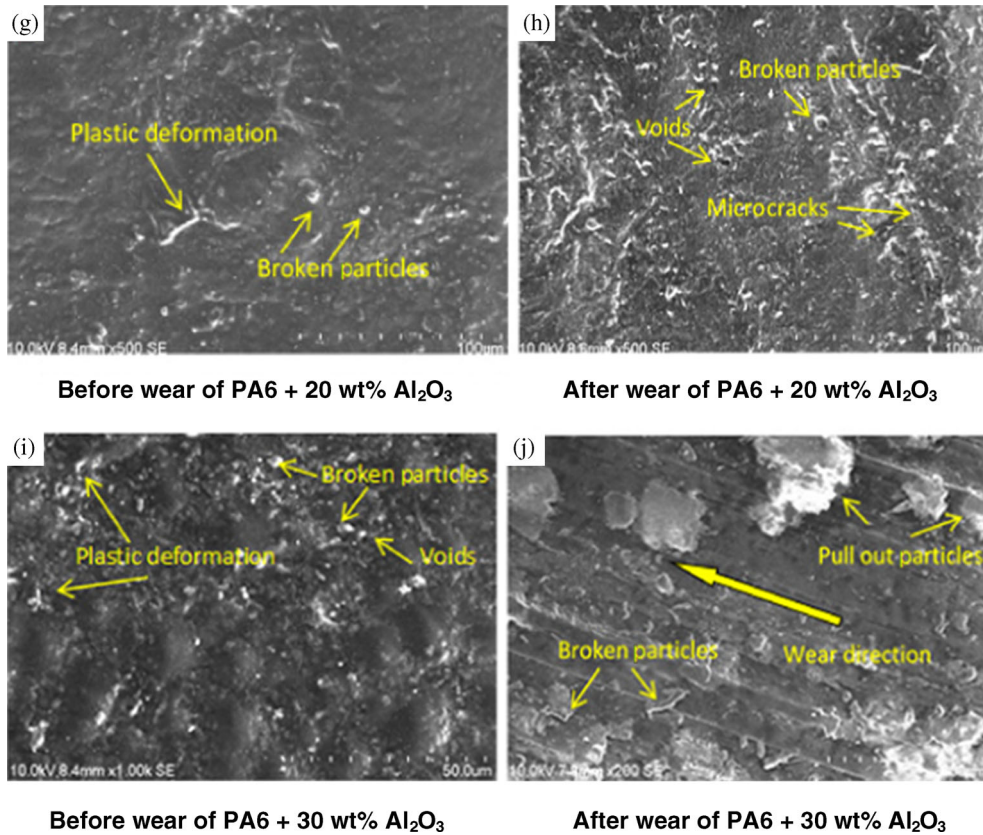


Figure 5. (Continued)

darker particles represent the graphite and the lighter ones are PA6. The bonding structure of PA6 and graphite particles are formed layer by layer, due to a small amount of graphite particles reinforced with PA6. Figure also shows the plastic deformation and broken particles on the surfaces of PA6. The bonding strength of graphite is clearly visible in figure 6d, which indicates the migration action and layer formation of graphite with PA6. However, the wear track formation on PA6 is clearly visible. Figure 6e reveals that the graphite particles gradually penetrate into the PA6 due to added graphite content by 10 wt%. Wedge formation and broken particles are also observed on the PA6 surfaces. While the amount of graphite particles is increased beyond 10% weight, there is some accumulation and cluster of the particles, as shown in figure 6f. The cluster formation occurs on the relative frictional surface. Also, it shows that plastic deformation and broken particles are found on the surface of PA6 with 10 wt% graphite. Here, the filler material dislocated due to maximum applied load and created higher friction on PA6. Figure 6g shows the uniform dispersion of graphite particles with PA6. However, 20 wt% graphite-reinforced PA6 displays the uniform distribution of graphite particles in PA6. We clearly observe a good interfacial bonding between graphite and polymer material matrix. Hence, voids, broken particles and wedge formation are not found on the surface of the PA6, but only plastic deformation was observed with 20 wt% graphite, as in figure 6g and h. The graphite has good bonding to

the polymer matrix and supports the load from the counter face effectively [18]. However, the surface morphology of graphite-reinforced PA6 composites is formed to display a very smooth pattern of PA6 with 20 wt% graphite (figure 6h). It reveals that the graphite particles strongly protect the top of the surface of the composite material under dry sliding test conditions. There are no crack formation, broken particles, wedge formation or any pullout of the particle signifying good bonding between the filler and the matrix material. Figure 6i and j shows the scanning electron microscopy (SEM) image of 30 wt% graphite-reinforced with PA6 composites. With further addition of graphite content, the worn surface of PA6/graphite is slightly smooth and there are some voids, broken particles, plastic deformation and microcracks, figure 6i, on the surface of PA6. The poor interfacial bonding is observed in figure 6j, due to the uneven distribution of graphite and improper mixing results PA6 detached from the graphite particles along with the voids, plastic deformation and microcracks on the PA6 composites. Figure 6c and j represents the graphite particles integrated on the PA6 composites and consequently the worn surface is protected from the wear and friction. This may be due to excellent self-lubricity of graphite that reduced the friction and wear of polymer composites [18].

The SEM images indicate that an adhesive wear is activated. The severity of the wear mechanism is reduced as graphite content increases. In the case of composite



containing 20 wt% graphite, the worn surface is very smooth and plastic deformation was observed (figure 6g and h). These observations indicate that the filler in small quantities was helpful for wear reduction as has been supported in the literature [19,20]. The worn surface of 30 wt% graphite-reinforced PA6 was characterized by severe voids, microcracks, broken particles and plastic deformation (figure 6i and j), which corresponds to its worse tribological properties. The plastic deformation and adhesive damage are created in the weaker part of the polymer and thus produce particles emission and wear [21]. Incorporating graphite contents into the polymer matrix changes the wear mechanism (figure 6g and h). The worn surface of the composite filled with 20 wt% graphite is characterized by slight plastic deformation.

In fact, less matrix wear damage can be identified. This signifies that the graphite particles incorporated in the PA6 polymer effectively act to restrain the direct contact between the polymer and the hard steel counterpart; subsequently, the friction and wear are seriously decreased, owing to their good solid-lubricating and easy shearing action [22].

### 3. Results and discussion

#### 3.1 Effect of applied load on friction co-efficient of $Al_2O_3$ composite specimens

Figures 7–10 show the variation of frictional force of PA6 and reinforced PA6 composites for different loads. The

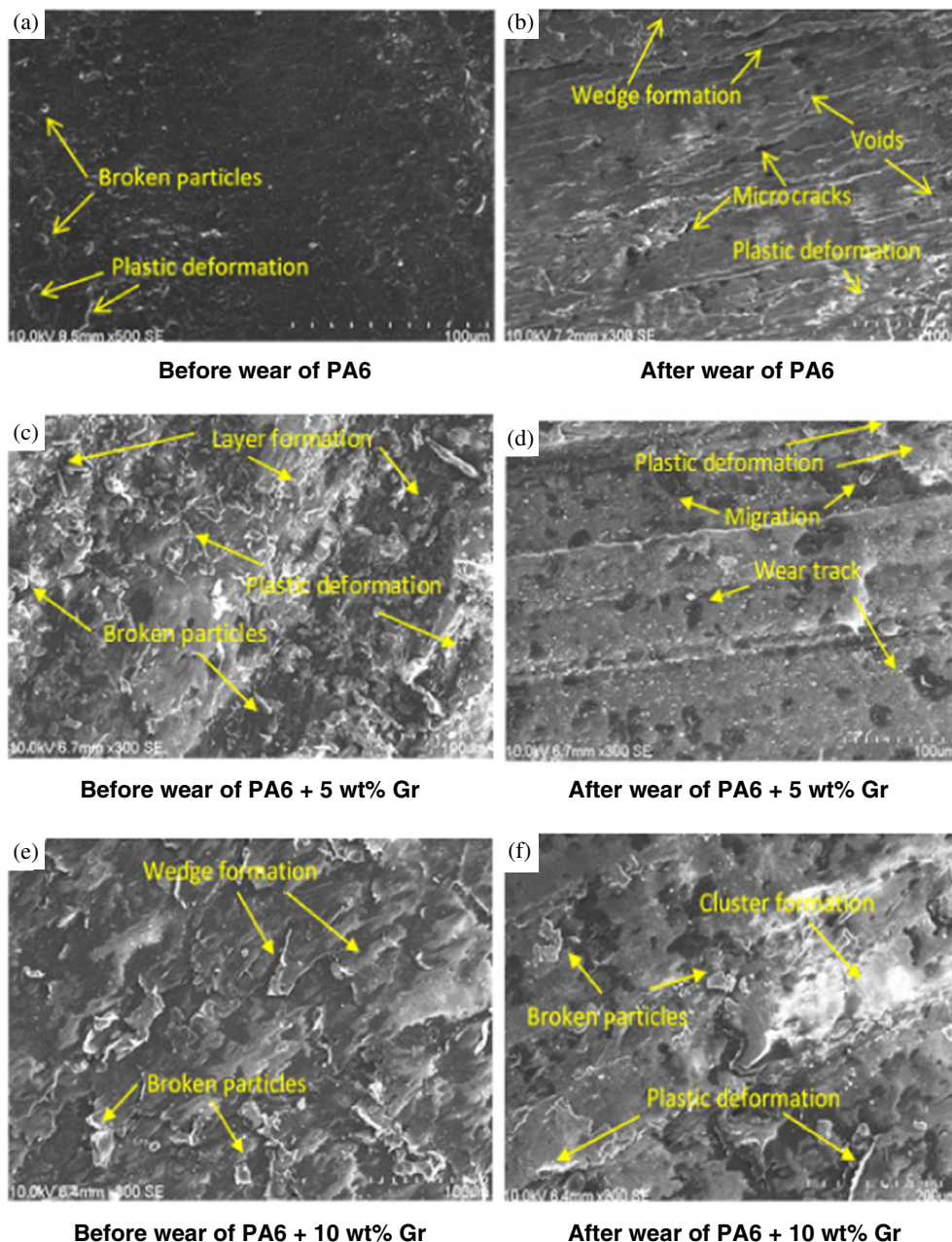


**Figure 6.** SEM images of PA6 and graphite-reinforced PA6 composites.

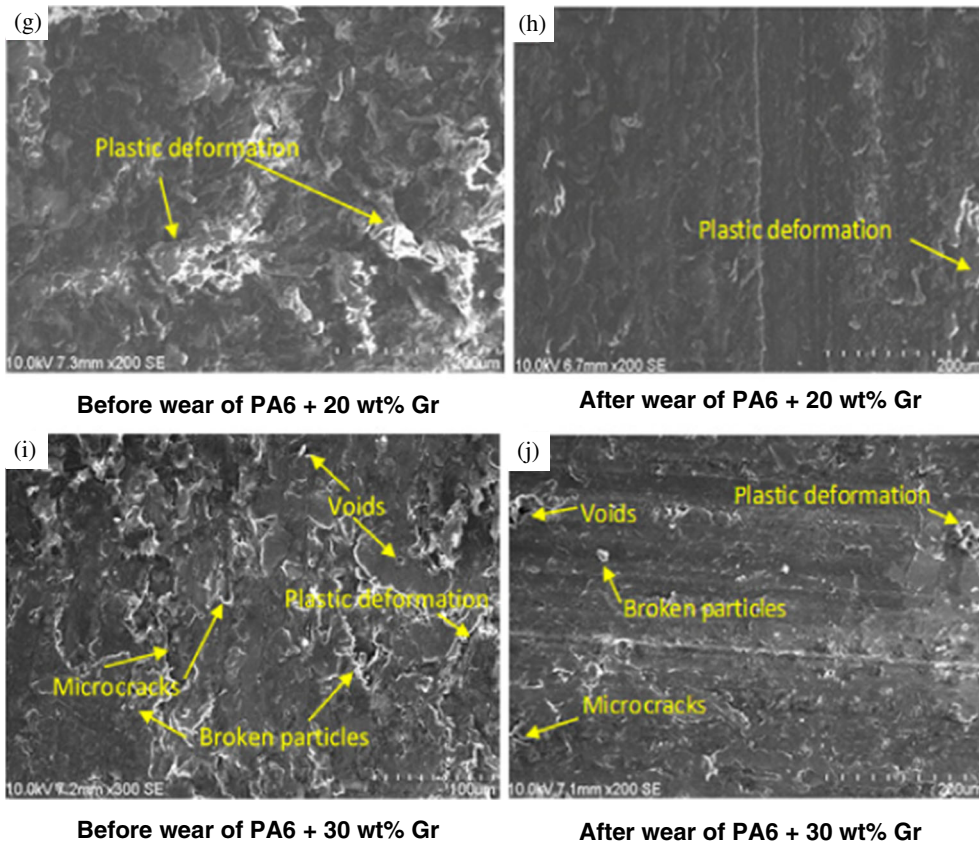


Figure 6. (Continued)

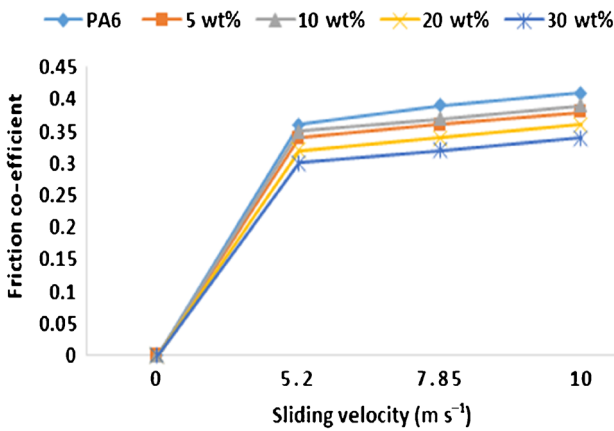


Figure 7. Friction co-efficient of 5 N load.

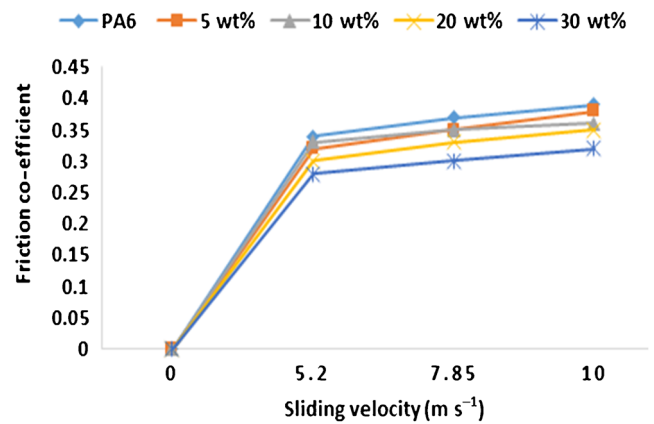


Figure 8. Friction co-efficient of 10 N load.

increase in friction co-efficient with an increase in load is attributed for the maximum sliding velocities at the different weight fractions of the reinforcement. It is revealed that the value of co-efficient of friction is low at initial loads for unreinforced PA6 and reinforced PA6 composites. It is found that the average co-efficient of frictions are in the range of 0.38 and 0.35 for PA6 with 5 wt% Al<sub>2</sub>O<sub>3</sub> composite, 0.36 and 0.33 for PA6 with 10 wt% Al<sub>2</sub>O<sub>3</sub> composite and the average co-efficient of frictions are in the range of 0.35 and 0.32 for PA6 with 20 wt% Al<sub>2</sub>O<sub>3</sub> composite. As a final point, the

average co-efficient frictions are in the range of 0.33 and 0.3 for PA6 with 30 wt% Al<sub>2</sub>O<sub>3</sub> composite. However, the average co-efficient of friction is 0.42 and 0.37 for unreinforced PA6 material. Although PA6 with 30 wt% of weight fraction has the lowest co-efficient of friction at any specific load, it is concluded that the increase of load indicates to an important increase in the friction co-efficient, as shown in figures 7–10. From this experiment, it is confirmed that the co-efficient friction of the composite PA6 with 30 wt% is low for all loads.



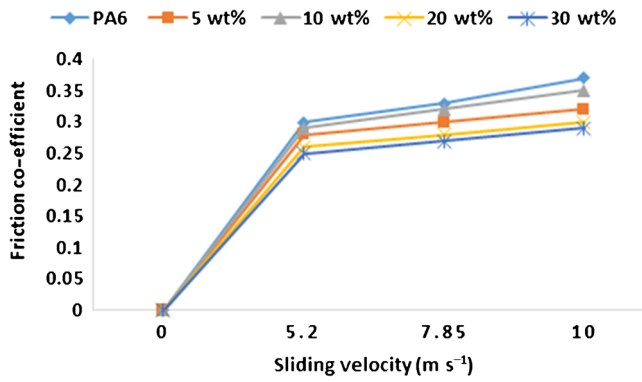


Figure 9. Friction co-efficient of 20 N load.

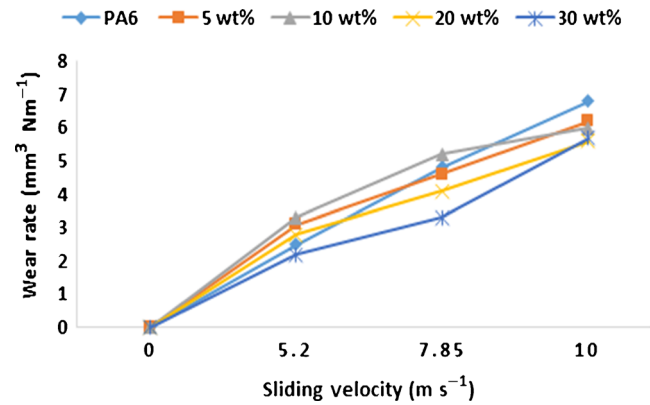


Figure 11. Wear rate of 5 N load.

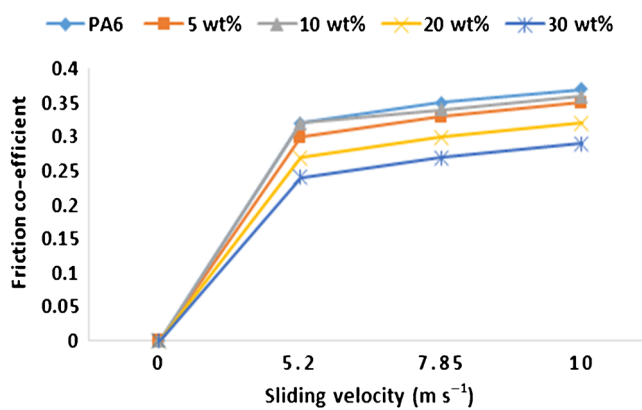


Figure 10. Friction co-efficient of 30 N load.

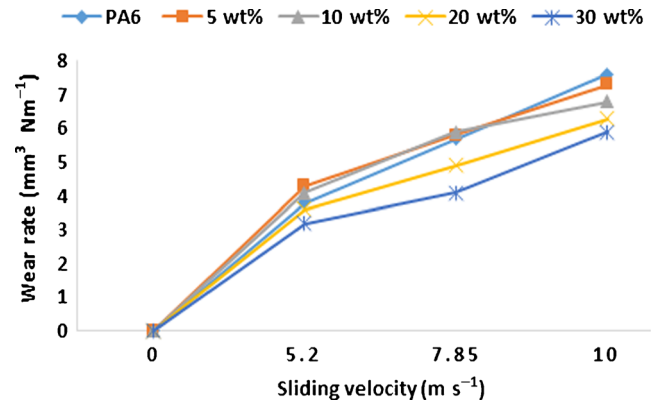


Figure 12. Wear rate of 10 N load.

### 3.2 Effect of applied load on wear rate of Al<sub>2</sub>O<sub>3</sub> composite specimens

The specific wear rate was calculated [11] using the following relation:

$$\text{Wear rate} = (\Delta m / \rho L d) \times 10^3 \text{ mm}^3 \text{ Nm}^{-1},$$

where  $\Delta m$  is the mass loss in grams,  $\rho$  the density of the test material in  $\text{g cm}^{-3}$ ,  $L$  the load in Newton and  $d$  the sliding distance in metres. The readings were plotted at a regular time interval of 5 min. The specimen surface was observed using a precision electronic balance with an accuracy of  $\pm 0.01$  mg. Figures 11–14 show the wear characteristics of the composites under 5, 10, 20 and 30 N loads. Applied load is one of the most important factors affecting the wear rate of composites. The wear rate of pure PA6 composite material does not influence varying load conditions. The wear rate of PA6 with 30 wt% Al<sub>2</sub>O<sub>3</sub> is lesser compared to pure PA6. The amount of wear decreased with increase in the content of alumina particles. This is because of Al<sub>2</sub>O<sub>3</sub> particles being strongly bonded with a base material; they protect the surface against severe destructive action by the counter face, because of the stronger interfacial bonding characteristics, which plays a vital role in transferring loads from the matrix to hard particles [23,24]. Moreover, Al<sub>2</sub>O<sub>3</sub> particles

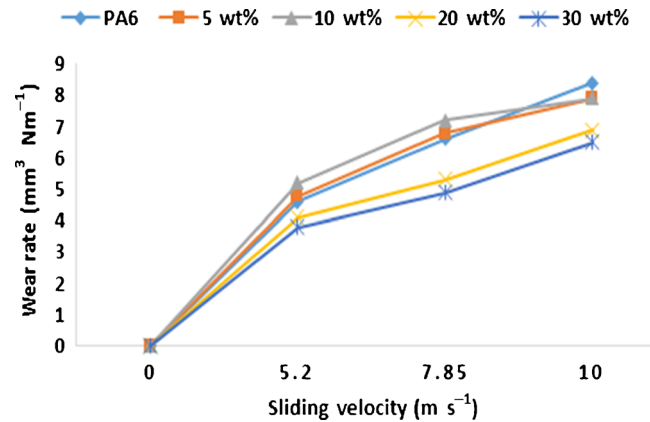


Figure 13. Wear rate of 20 N load.

have substantially improved the wear resistance. However, the results in figure 13 show that the PA6 reinforced 30 wt% Al<sub>2</sub>O<sub>3</sub> wear rate was reduced obviously compared with unreinforced PA6 and other composites. The wear resistance of the composites increases with increase in the percentage of Al<sub>2</sub>O<sub>3</sub> particles, as represented in figures 11–14. The co-efficient of friction of composites decreases with increase in the content of Al<sub>2</sub>O<sub>3</sub> reinforcement of particles, as indicated in figures 7–10. In wear test, the specimen contacts with the

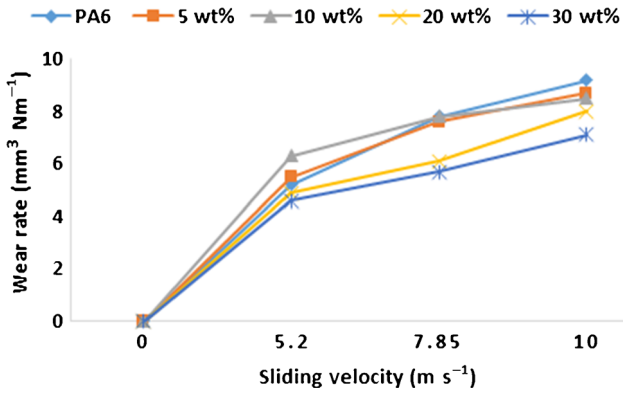


Figure 14. Wear rate of 30 N load.

disc and the important properties of heat and wear are produced on the contact surface of the specimen. The sliding contact of two materials results in heat generation at asperities and hence increases the temperature [25].  $\text{Al}_2\text{O}_3$  particles have a high hardness of  $1100 \text{ kg mm}^{-2}$  [26] and high thermal conductivity ( $30 \text{ Wm}^{-1} \text{ K}^{-1}$ ) [27]. Hence it has reinforced with PA6 and the characteristics of PA6 have been increased. Here, the  $\text{Al}_2\text{O}_3$  particles dispersed on the PA6 specimen, hence the characteristics of friction and wear have been protected from the contact surface.

The wear results (figures 11–14) indicate the average wear rate in the range of  $8.8 \times 10^{-3}$  and  $6.3 \times 10^{-3} \text{ mm}^3 \text{ Nm}^{-1}$  for PA6 with 5 wt%  $\text{Al}_2\text{O}_3$  composite,  $8.4 \times 10^{-3}$  and  $6 \times 10^{-3} \text{ mm}^3 \text{ Nm}^{-1}$  for PA6 with 10 wt%  $\text{Al}_2\text{O}_3$  composite,  $7.9 \times 10^{-3}$  and  $5.8 \times 10^{-3} \text{ mm}^3 \text{ Nm}^{-1}$  for PA6 with 20 wt%  $\text{Al}_2\text{O}_3$  composite, and  $7.1 \times 10^{-3}$  and  $5.9 \times 10^{-3} \text{ mm}^3 \text{ Nm}^{-1}$  for PA6 with 30 wt%  $\text{Al}_2\text{O}_3$  composite. Hence, PA6 with 30 wt%  $\text{Al}_2\text{O}_3$  composite formed high wear resistance and low co-efficient of friction on the surface compared with PA6 and other proportions.

Usually, the  $\text{Al}_2\text{O}_3$  particles have significantly improved hardness and wear resistance. Therefore, PA6-reinforced 30 wt%  $\text{Al}_2\text{O}_3$  had a low co-efficient of friction and low wear rate of  $7.1 \times 10^{-3} \text{ mm}^3 \text{ Nm}^{-1}$ . However, the results in figure 14 show that PA6-reinforced 30 wt%  $\text{Al}_2\text{O}_3$  wear rate was reduced obviously compared with PA6 and other composites.

In wear test, the specimen contacts with the disc and the important properties of heat and wear are produced on the contact surface of the specimen.  $\text{Al}_2\text{O}_3$  particles have high hardness and high thermal conductivity; hence, when reinforced with PA6 the characteristics of PA6 get increased. Here, the particles dispersed on the PA6 specimen contact with the disc and the characteristics of heat and wear have been protected from the contact surface of the tribometer. Hence it has produced high wear resistance and minimum heat generation on the surface.

### 3.3 Effect of applied load on friction co-efficient of graphite composite specimens

Figure 15 shows the variation of frictional co-efficient of PA6 and graphite-reinforced PA6 composites for different loads.

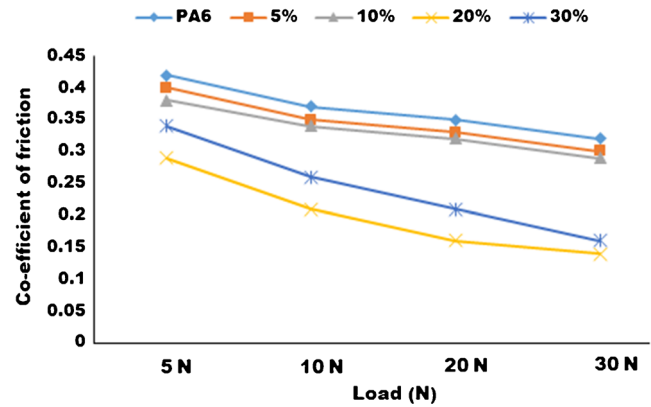


Figure 15. Variations of the friction co-efficient for PA6 and graphite/PA6 composites.

The decrease in friction co-efficient with an increase in load is attributed because of maximum sliding velocities at the different weight fraction of reinforcement. The graphite reinforced PA6 composite materials have the lower frictional co-efficient as compared to pure PA6. However, it was observed during the experiment that the composite material shows a slight change in frictional co-efficient with the variation of load and sliding velocity. The average co-efficient of frictions are in the range of 0.4 and 0.3 for PA6 with 5 wt% graphite composite, 0.38 and 0.29 for PA6 with 10 wt% graphite composite and the average co-efficient of frictions in the range of 0.29 and 0.14 for PA6 with 20 wt% graphite composite. As a final point, the average co-efficient frictions are in the range of 0.34 and 0.16 for PA6 with 30 wt% graphite composite. However, the average co-efficient of friction is 0.42 and 0.37 for pure PA6 material. There is a significant reduction in the friction co-efficient at graphite weight content as low as PA6 with 20 wt% graphite. Taking all these results into consideration, it was understood that the presence of graphite appeared to make effects on the friction co-efficient for the PA6. This is consistent with the results reported in ref. [10]. In addition, PA6 with a content of graphite 20 wt% showed the lowest co-efficient of friction among the composites tested in this study. Figure 15 shows the variation of co-efficient of friction with time. It is obvious that the friction co-efficient increases initially to a higher value due to the fresh abrasive material, and as the process continues it nearly remains same for the entire test period. It is also noted that the co-efficient of friction decreases when the filler content increases, because of the lubricating property of the graphite filler. Also 20 wt% graphite content had the least value for the co-efficient of friction.

### 3.4 Effect of applied load on wear rate of graphite composite specimens

During initial tests, the surfaces of both the specimens and the steel counterparts were rough and thus strong interconnections between the surfaces resulted in a high friction co-efficient. As the wear process continued, the rough profiles of

the steel counterparts and the specimens were smoothed. When the applied load is small, the stress in the contact region between the specimen and the counterpart is small, the frictional heat is also less. With the increase in sliding velocity, the friction heat is much more, additional wear debris adheres on the specimen.

Figure 16 shows the wear characteristics of PA6, graphite-reinforced PA6 composites under 5, 10, 20 and 30 N loads. Applied load is one of the most important factors affecting the wear rate of composites. The wear rate was gradually decreased while increasing the load. Figure 16 shows the influence of load on the specific wear rate of the composites. The specific wear rate decreases with the normal load. The specific wear rate was relatively high at the load of 5 N because of less dispersion and fewer amounts of abrasive particles in action with the rubbing surface. The abrasion wear greatly increased at higher loads, because most of the abrasive particles penetrated into the surface and produced more broken particles and voids, resulting in more material removal by a severe plastic deformation. In wear test, the specimen contacts with the disc and produced heat and wear on the contact surface of the specimen. The average wear rate was in the range of  $7.5 \times 10^{-3}$  and  $4.9 \times 10^{-3} \text{ mm}^3 \text{ Nm}^{-1}$  for PA6 with 5 wt% graphite composite,  $7.2 \times 10^{-3}$  and  $4.5 \times 10^{-3} \text{ mm}^3 \text{ Nm}^{-1}$  for PA6 with 10 wt% graphite composite,  $5.8 \times 10^{-3}$  and  $3.7 \times 10^{-3} \text{ mm}^3 \text{ Nm}^{-1}$  for PA6 with 20 wt% graphite composite and  $6.3 \times 10^{-3}$  and  $4.1 \times 10^{-3} \text{ mm}^3 \text{ Nm}^{-1}$  for PA6 with 30 wt% graphite composite. However, the average wear rate is  $9.2 \times 10^{-3}$  and  $6.8 \times 10^{-3} \text{ mm}^3 \text{ Nm}^{-1}$  for pure PA6 material. Hence, PA6 with 20 wt% graphite composite formed high wear resistance and low co-efficient of friction on the surface compared with PA6 and other proportions.

The amount of wear decreased with increase in the content of graphite particles. When the hard particles are strongly bonded to a base material, they protect the surface against severe destructive action by the counter face, because of the stronger interfacial bonding characteristics, which play a vital role in transferring loads from the matrix to the graphite particles. The graphite particles have substantially improved the wear resistance. The wear rate decreases with the addition

of graphite powder up to 20%. The optimum value of specific wear rate was obtained for the composite with 20% graphite content. Increasing the graphite content contribute to a negative effect on the wear and friction co-efficient properties of this composite. Graphite particles have high compressive strength, thermal conductivity and excellent lubricity. Hence, graphite has reinforced with PA6 and the characteristics of PA6 have been increased. Here, the graphite particles dispersed on the PA6 specimen contact with the disc and the characteristics of friction and wear have been protected from the contact surface of the tribometer.

### 3.5 Comparison of wear loss for PA6 and graphite/PA6 composites

Figure 17 shows the wear loss characteristics of PA6 and graphite-reinforced PA6 composites under the applied loads of 5, 10, 20 and 30 N. Applied load is one of the most important factors affecting the wear rate of composites. The average wear loss was in the range of 3.336–3.325 g for PA6 with 5 wt% graphite composite, 3.330–3.322 g for PA6 with 10 wt% graphite composite, 3.327–3.320 g for PA6 with 20 wt% graphite composite, 3.347–3.331 g for PA6 with 30 wt% graphite composite and 3.342–3.328 g for PA6 with 40 wt% graphite composite.

The highest wear loss occurred in pure PA6, whereas PA6 with 20 wt% graphite composite material exhibited lesser wear loss. The amount of wear decreased with increase in the content of graphite particles [28]. When the particles are strongly bonded to the base material, they protect the surface against severe destructive action by the counter face and plays a vital role in transferring loads from the matrix to graphite particles [6,7].

Figure 6 clearly shows that PA6 reinforced with graphite 20 wt% has a low wear loss compared with other proportions. PA6/20 wt% graphite content compared with PA6 had reduced wear loss by 76.66%. This suggests that the incorporation of graphite in PA6 significantly reduced wear rate compared with PA6. The sliding contact of two materials results in heat generation at asperities and hence increases

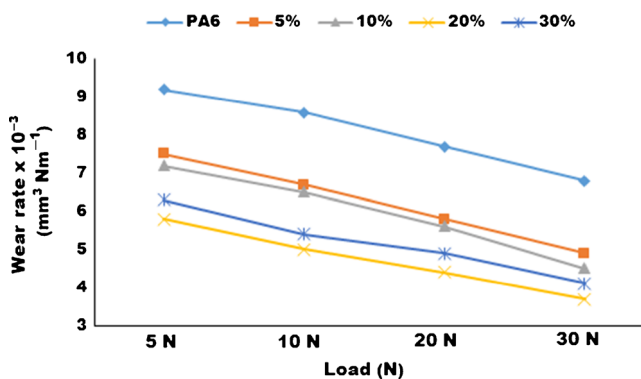


Figure 16. Variations of the wear rate for PA6 and PA6/Gr composites.

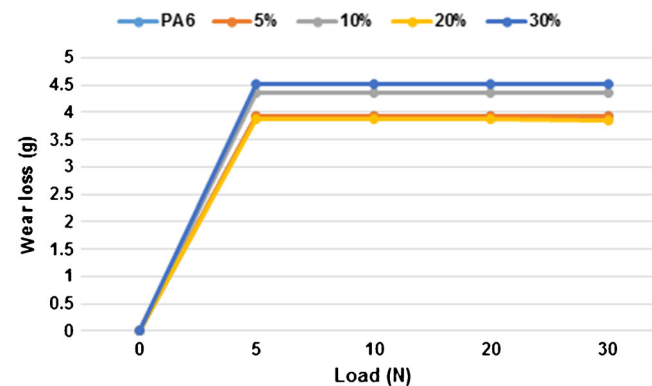


Figure 17. Variations of the wear loss for PA6 and PA6/Gr composites.



the temperature [28]. The heat dissipation rate is gradually increased due to the reinforcement of graphite with PA6 [29]. During wear test, heat generated between the contact surfaces. The accumulated heat of the material should be dissipated properly. Otherwise, it would lead to negative effect. Graphite particles have an excellent antifriction characteristic that dissipate the heat from the contact surface gradually.

3.6 Heat calculation

If the load is increased at a higher velocity, it is known that the surface of polymers melt at a certain load because of friction heating. Normally, the heat generation occurs in sliding between the materials and temperature increases between the two friction surfaces. The amount of heat generated can be determined by  $H = \mu PV$  (Watts), where  $\mu$  is the co-efficient of friction,  $P$  the applied load and  $V$  the sliding velocity. The calculated values for heat generated during wear tests for the loads 5, 10, 20 and 30 N and for various speeds 1000, 1500 and 2000 r.p.m. are shown in tables 3 and 4. As compared to PA6, the composite material showed lower interfacial temperature due to the high thermal conductivity of the filler materials. Figure 18 shows the variation of heat generation in various loading condition for PA6 and Al<sub>2</sub>O<sub>3</sub>/graphite-reinforced PA6 composites.

3.7 Surface roughness test

The wear tested samples were subjected to the surface roughness test by using a Mitutoyo, SJ210 tester, Spectrum Scientific Company, Chennai. The reason for using the surface

roughness test is to find out the influences of Al<sub>2</sub>O<sub>3</sub> and graphite particles on the surface roughness performance of the PA6 composite specimen. The condition of surfaces and roughness measurement are shown in table 5.

The measured worn surface roughness of various composites for the 30 N load is given in table 5. From table 5, it is obvious that the surface roughness value is higher for the pure PA6, and the roughness value decreases with an increase in the percentage of Al<sub>2</sub>O<sub>3</sub> and graphite reinforcement. It is obvious that the curve varies linearly up to 30 wt% Al<sub>2</sub>O<sub>3</sub>/PA6. Similarly, the curve varies linearly up to 20 wt% graphite/PA6. Then, the curve decreases slowly with a further increase in the percentage of graphite. A graph was plotted between the various weight percentages of Al<sub>2</sub>O<sub>3</sub> and

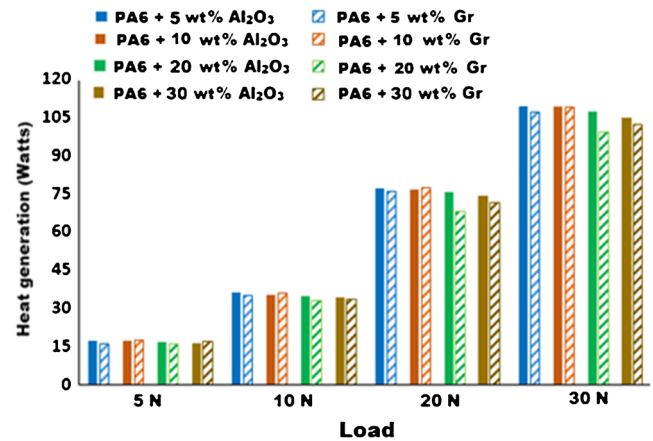


Figure 18. Comparison of heat generation for Al<sub>2</sub>O<sub>3</sub>- and graphite-reinforced PA6 composites.

Table 3. Heat generation (Watts) for PA6 and Al<sub>2</sub>O<sub>3</sub>/PA6 composite specimens.

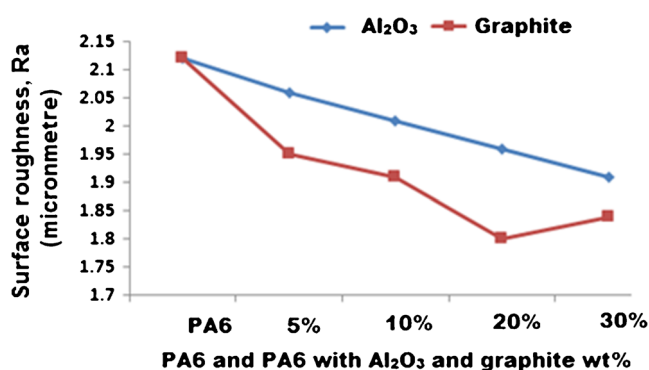
Test specimen	Load 5 N			Load 10 N			Load 20 N			Load 30 N		
	Sliding velocity (m s <sup>-1</sup> )			Sliding velocity (m s <sup>-1</sup> )			Sliding velocity (m s <sup>-1</sup> )			Sliding velocity (m s <sup>-1</sup> )		
	5.23	7.85	10	5.23	7.85	10	5.23	7.85	10	5.23	7.85	10
PA6	7.8	12.9	18.5	19.7	27.4	37	39.5	58	78	86.4	91.8	113
PA6 + 5 wt% Al <sub>2</sub> O <sub>3</sub>	7.6	12.3	17.4	19.1	26.9	36.2	38.3	56.7	77.2	85.6	90.3	111
PA6 + 10 wt% Al <sub>2</sub> O <sub>3</sub>	7.5	11.8	17.0	18.7	26.4	35.4	37.9	56.1	76.8	85.1	89.8	109
PA6 + 20 wt% Al <sub>2</sub> O <sub>3</sub>	7.2	11.3	16.8	18.2	26.1	34.8	35.8	55.8	75.7	84.6	88.6	107
PA6 + 30 wt% Al <sub>2</sub> O <sub>3</sub>	7.0	11.1	16.2	17.6	25.7	34.1	34.3	54.5	74.2	83.9	87.1	105

Table 4. Heat generation (Watts) for PA6 and graphite/PA6 composite specimens.

Test specimen	Load 5 N			Load 10 N			Load 20 N			Load 30 N		
	Sliding velocity (m s <sup>-1</sup> )			Sliding velocity (m s <sup>-1</sup> )			Sliding velocity (m s <sup>-1</sup> )			Sliding velocity (m s <sup>-1</sup> )		
	5.23	7.85	10	5.23	7.85	10	5.23	7.85	10	5.23	7.85	10
PA6	7.8	12.9	18.5	19.7	27.4	37	39.5	58	78	86.4	91.8	113
PA6 + 5 wt% graphite	7.3	11.7	16	18.6	25.9	35	36.4	54.9	76	83.3	89.7	107
PA6 + 10 wt% graphite	7.5	12.5	17.5	19.2	26.6	36	37.7	55.3	77.3	84.9	90.7	109
PA6 + 20 wt% graphite	6.7	11	16	17.1	25.9	32.8	33.3	51.8	68	80.2	84	99
PA6 + 30 wt% graphite	6.9	11.3	15.4	14.6	24	33.4	34.9	53.6	71.5	82.7	85.3	102

**Table 5.** Worn surface roughness of various composites (30 N load).

Polymer materials composition	Surface roughness (Ra) in $\mu\text{m}$	Nature of surface condition
PA6	2.12	Smooth
PA6 + 5 wt% $\text{Al}_2\text{O}_3$	2.06	Smooth
PA6 + 10 wt% $\text{Al}_2\text{O}_3$	2.01	Smooth
PA6 + 20 wt% $\text{Al}_2\text{O}_3$	1.96	Fine smooth
PA6 + 30 wt% $\text{Al}_2\text{O}_3$	1.91	Fine smooth
PA6 + 5 wt% graphite	1.95	Fine smooth
PA6 + 10 wt% graphite	1.91	Fine smooth
PA6 + 20 wt% graphite	1.80	Fine smooth
PA6 + 30 wt% graphite	1.84	Fine smooth

**Figure 19.** Surface roughness of various weight percentage for  $\text{Al}_2\text{O}_3$  and graphite composites.

graphite-reinforced PA6 composites vs. surface roughness, as shown in figure 19.

**3.7a Effect of surface roughness:** For the reinforced polymers, the surface roughness decreased with increase in the content of  $\text{Al}_2\text{O}_3$  in PA6. The surface roughness drastically decreased while adding graphite in PA6. The variation of surface roughness for  $\text{Al}_2\text{O}_3$  and graphite-reinforced polymer composites is indicated in figure 19. It is not expected to be greater than that of the unfilled PA6, the reason for the apparently lower sensitivity of this material for the mating surface roughness is also in contradiction with available engineering strategies [30–33]. The lower sensitivity of PA6 + 30 wt%  $\text{Al}_2\text{O}_3$  appears to be related to the ease with which a wear layer is formed. In the present experiments, PA6 + 30 wt%  $\text{Al}_2\text{O}_3$  was found to form a wear layer at low roughness value (1.91  $\mu\text{m}$ ). The formation of a wear layer may be expected to decrease the abrasive effect of the mating surface roughness, reducing the surface roughness. Similarly, PA6 + graphite composites had fine smooth effect. It is well-known that graphite materials have a good lubricity effect on steel material, reducing the surface roughness on the PA6 + graphite composite specimens.

### 3.8 Thermogravimetric analysis

The thermal decomposition studies were performed over a temperature range of 50–600°C using an EXSTAR TG/DTA 6300, Hitachi, Japan, under both nitrogen and air environments at the temperature between 27 and 700°C  $\text{min}^{-1}$ . The heating rate was maintained at 10°C. The temperature and the weight scales were calibrated using high-purity standards (Nickel and Iron) over a specific range of heating rates with a calibration parameter of their respective Curie points.

**3.8a Thermal stability of  $\text{Al}_2\text{O}_3$ :** Thermogravimetric analysis (TGA) measures the loss of weight in material as a function of temperatures (or time) under a controlled atmosphere to determine the thermal stability and composition. Thermal degradation profiles of the optimally reinforced PA6/30 wt%  $\text{Al}_2\text{O}_3$  composites were determined from the TG and differential thermal analysis (DTA) thermogram, as represented in figure 20. As expected the two stages of degradation are evident in both the profiles, which corresponded to temperature regions for different constituents like moisture evaporation (upto 100°C) and degradation of the material of  $\text{Al}_2\text{O}_3$  (200–500°C). The depolymerization of  $\text{Al}_2\text{O}_3$  usually occurs between 400 and 500°C.

The initial peak at 90°C in raw for the  $\text{Al}_2\text{O}_3$  data obviously represent the loss of moisture and other volatiles at the first degradation, which is observed between room temperature and 100°C. Further, the next peak which was seen around 450.9°C denotes DTA degradation of  $\text{Al}_2\text{O}_3$  and a prominent peak appears at the temperature corresponding to the maximum degradation rate. Moreover, optimal  $\text{Al}_2\text{O}_3$  reinforced with PA6 composites increases the degradation temperature (400–500°C), which is due to retention and improvement of the structural order and reduction in the amorphous content. A greater crystalline structure essentially requires a higher degradation temperature, which is clearly evident in optimal alumina reinforced with PA6 composites. The derivative thermogravimetric (DTG) curve displays the decomposition temperature of  $\text{Al}_2\text{O}_3$  composite material value of above 410°C.

**3.8b Thermal stability of graphite:** Thermal degradation profiles of the optimally reinforced PA6/20 wt% graphite composites were determined from the TG and DTA thermogram, as represented in figure 21. As expected the two stages of degradation are evident in both the profiles, which corresponded to temperature regions for different constituents like moisture evaporation (up to 100°C) and degradation of the material of graphite (200–600°C). The depolymerization of graphite usually occurs between 450 and 550°C. The initial peak at 110°C in raw for the graphite data obviously represent the loss of moisture and other volatiles at the first degradation, which is observed between room temperature and 100°C. Further, the next peak that was seen around 466.7°C denotes DTA degradation of graphite and a prominent peak appears at the temperature corresponding to

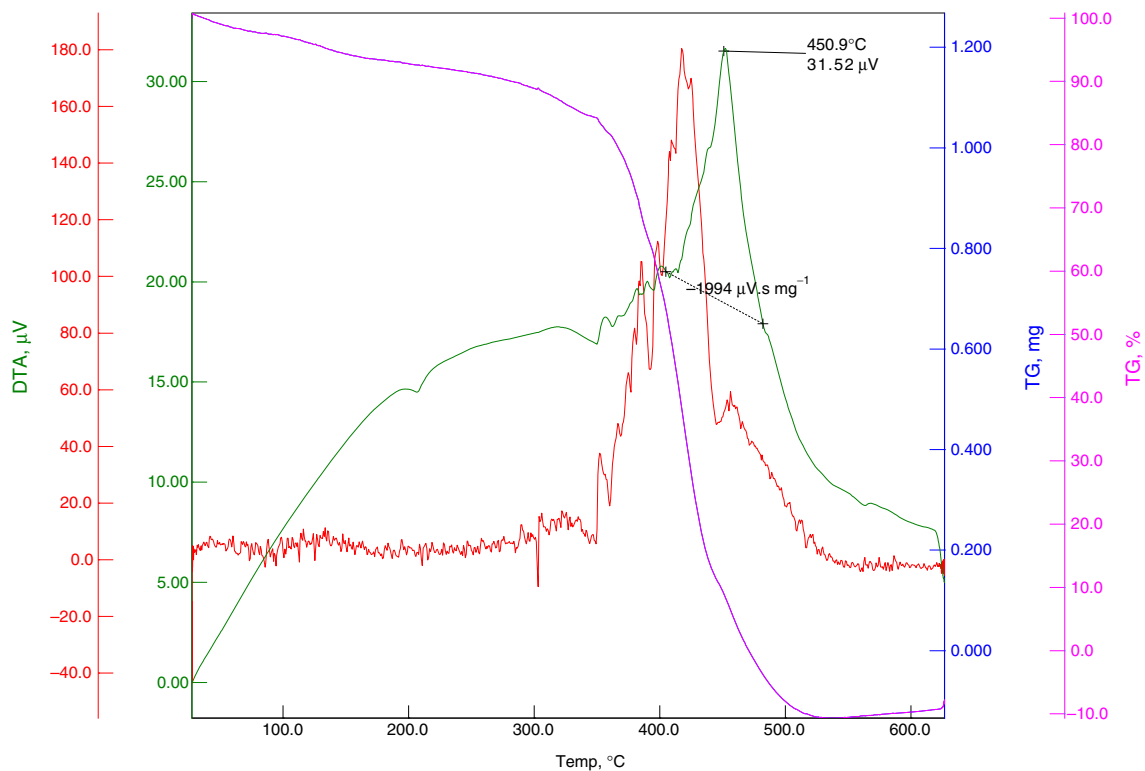


Figure 20. TGA thermogram of the PA6 + 30 wt% Al<sub>2</sub>O<sub>3</sub>.

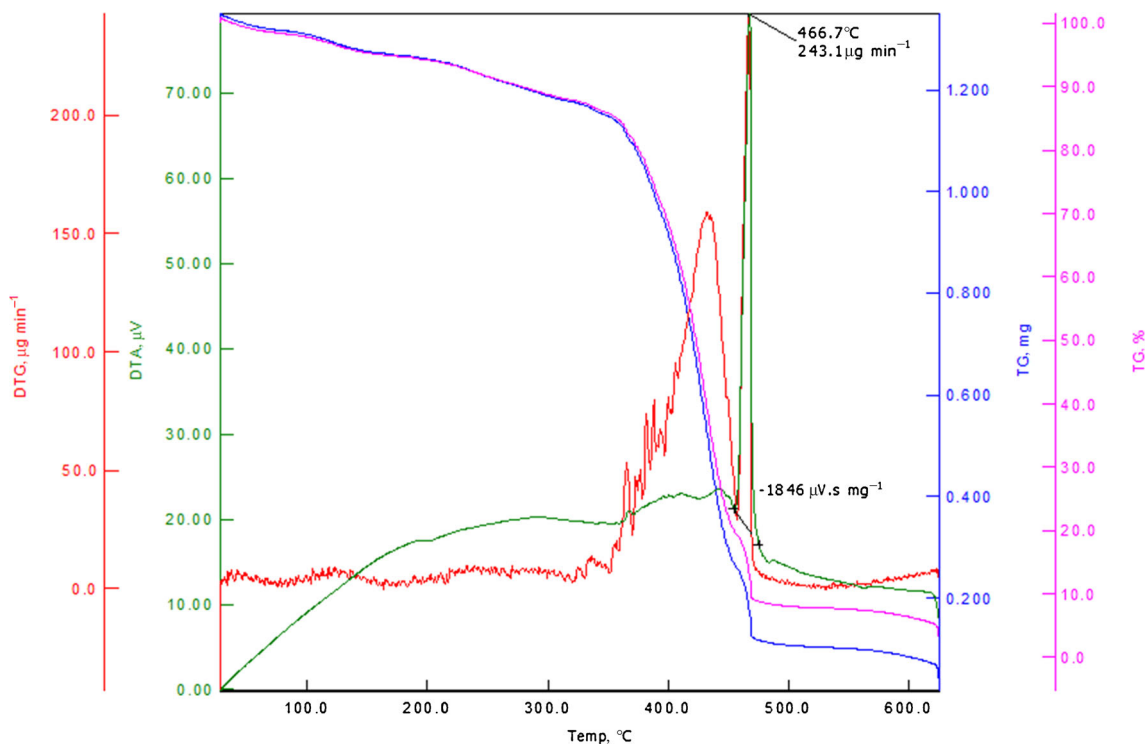


Figure 21. TGA thermogram of the PA6 + 20 wt% Gr.

the maximum degradation rate. Moreover, optimal graphite reinforced with PA6 composites increases the degradation temperature (400–600°C), which is due to retention and

improvement of the structural order and reduction in the amorphous content. Greater crystalline structures essentially require a higher degradation temperature, which is clearly



evident in optimal graphite reinforced with PA6 composites. The DTG curve displays the decomposition temperature of graphite composite material value of above 440°C.

#### 4. Conclusion

In this study, PA6 blended with Al<sub>2</sub>O<sub>3</sub> and graphite composites were prepared by injection moulding machine. The effect of Al<sub>2</sub>O<sub>3</sub> and graphite content of the tribological properties of PA6 material was inspected under room temperature by conducting wear and surface roughness tests. Thermal stability of Al<sub>2</sub>O<sub>3</sub> and graphite particles were studied through TGA test. SEM was utilized to examine the worn surface microstructures and wear mechanisms before and after the tribological test. The possibility of improving the tribological properties of PA6 by the additions of Al<sub>2</sub>O<sub>3</sub> and graphite in various weight proportions were studied. From the experimental analysis, the following conclusions are made:

1. The friction co-efficient downgraded up to 21.42% for PA6 + 30 wt% Al<sub>2</sub>O<sub>3</sub> and 30.9% for PA6 + 20 wt% graphite composites compared with PA6.
2. The wear resistance significantly enhanced up to 22.82% for PA6 + 30 wt% Al<sub>2</sub>O<sub>3</sub> and 36.9% for PA6 + 20 wt% graphite composites compared with PA6.
3. The surface roughness value decreases with an increase in the percentage of the Al<sub>2</sub>O<sub>3</sub> and graphite reinforcement.
4. PA6 + 30 wt% Al<sub>2</sub>O<sub>3</sub> and PA6 + 20 wt% graphite shows reduced surface roughness values compared to PA6 and other PA6 composites.
5. Heat generation was degraded up to 7.07% for PA6 + 30 wt% Al<sub>2</sub>O<sub>3</sub> and 12.3% for PA6 + 20 wt% graphite composites compared with PA6.
6. According to TGA, the weight loss in composites was influenced by filler loading. However, the loss was significant only in the high temperature region (PA6+ 30 wt% Al<sub>2</sub>O<sub>3</sub> for 450.9°C and PA6 + 20 wt% graphite for 466.7°C).
7. A significant decrease of the wear, friction co-efficient and the heat generation takes place with the addition of Al<sub>2</sub>O<sub>3</sub> and graphite to the PA6 polymer.
8. Addition of 30 wt% of Al<sub>2</sub>O<sub>3</sub> improved the friction co-efficient behaviour and the wear abilities of the PA6 polymer.

The tribological study conducted in this study revealed that the improved tribological behaviours are due to the addition of Al<sub>2</sub>O<sub>3</sub> and graphite. Due to the stronger interfacial bonding characteristics of Al<sub>2</sub>O<sub>3</sub> and graphite conformed to morphological test and showed improvement in the wear resistance. The PA6 composites tested in this study may find useful applications in fabrication of plastic gears for lightly loaded drives with high level of wear resistance and durability. They transmit power quietly and often without lubrication in applications such as food processors, windshield wiper drives and even watches.

#### References

- [1] Watanabe Makoto and Haruchiyo Yamaguchi 1986 *Wear* **110** 379
- [2] Tanaka Kyuichiro 1982 *Wear* **75** 183
- [3] Bahadur S and Tabor D 1985 *Polym. Wear Control* **287** 253
- [4] Hooke C J, Kukureka S N, Liao P, Rao M and Chen Y K 1996 *Wear* **200** 83
- [5] Kukureka S N, Hooke C J, Rao M, Liao P and Chen Y K 1999 *Tribol. Int.* **32** 107
- [6] Palabiyik M and Bahadur S 2000 *Wear* **246** 149
- [7] Palabiyik M and Bahadur S 2002 *Wear* **253** 369
- [8] Liu C Z, Wu J Q, Li J Q, Ren L Q, Tong J and Arnell A D 2006 *Wear* **260** 109
- [9] Jia B B, Li T S, Liu X J and Cong P H 2007 *Wear* **262** 1353
- [10] Cong P, Xiang F, Liu X and Li T 2008 *Wear* **265** 1106
- [11] Li D X, Deng X, Wang J, Yang J and Li X 2010 *Wear* **269** 262
- [12] Liu S P, Hwang S S, Yeh J M and Hung C C 2011 *Int. Commun. Heat Mass Transfer* **38** 37
- [13] Unal H and Mimaroglu A 2012 *Wear* **289** 132
- [14] Pogačnik A and Kalin M 2012 *Wear* **290** 140
- [15] Pan B, Zhang S, Li W, Zhao J, Liu J, Zhang Y and Zhang Y 2012 *Wear* **294** 395
- [16] Li D X, You Y L, Deng X, Li W J and Xie Y 2013 *Mater. Des.* **46** 809
- [17] Shaofeng Zhou, Qiaoxin Zhang, Chaoqun Wu and Jin Huang 2013 *Mater. Des.* **44** 493
- [18] Konieczny J, Chmielnicki B and Tomiczek A 2013 *J. Achiev. Mater. Manuf. Eng.* **60** 23
- [19] Wang Q, Zhang X and Pei X 2010 *Mater. Des.* **31** 3761
- [20] Suresha B, Chandramohan G, Renukappa M N and Siddaramaiah 2007 *J. Appl. Polym. Sci.* **103** 2472
- [21] Guo Q and Luo W 2001 *Wear* **249** 924
- [22] Zhang X, Liao G, Jin Q, Feng X and Jian X 2008 *Tribol. Int.* **41** 195
- [23] Qian X, Song L, Tai Q, Hu Y and Yuen R K K 2013 *Compos. Sci. Tech.* **74** 228
- [24] Jia Z, Hao C, Yan Y and Yang Y 2015 *Wear* **338** 282
- [25] Demir Z 2013 *Bull. Mater. Sci.* **36** 341
- [26] Barnes C, Shrotriya P and Molian P 2007 *Int. J. Machine Tools Manuf.* **47** 1864
- [27] Michálek M, Sedláčeka J, Parchovianskyb M, Michálková M and Galusek D 2014 *Ceram. Int.* **40** 1289
- [28] Li M, Wan Y, Gao Z, Xiong G, Wang X, Wan C and Luo H 2013 *Mater. Des.* **51** 257
- [29] Shin M W, Kim S S and Jang H 2011 *Trib. Lett.* **44** 151
- [30] Lancaster J K 1995 In: M J Neale (ed) *The tribology handbook*, 2nd edn (Oxford: Butterworth-Heinemann)
- [31] NCT polymer materials for bearing surfaces selection and performance Guide 1983, National Centre of Tribology, Risley, Warrington, UK
- [32] ESDU data item 87007 1987 Design and material selection for dry rubbing bearings, Tribology Series, Vol. 8, Engineering Sciences Data Unit International, London
- [33] Ramnath B V, Elanchezian C, Jaivignesh M, Rajesh S, Parswajinan C and Ghias A S A 2014 *Mater. Des.* **58** 332